Journal of Marine Technology and Environment
DOI:10.53464/JMTE.02.2026.08
ISSN (Print): 1844-6116
ISSN (Online): 2501-8795
https://www. jmte.eu

# REDUCTIONS IN ENGINE EXHAUST EMISSIONS IN A HYBRID FLETTNER ROTOR POWER-ASSISTED VESSEL

**Lubomir A. RIBAROV**[1]

[1]United States Merchant Marine Academy, Department of Marine Engineering, 300 Steamboat Road, Kings Point, NY 11027, USA, e-mail ribarovl@usmma.edu

***Abstract :*** With the increase of Greenhouse Gas (GHG) emissions, the maritime industry has seen an influx of low emission and environmental protection solutions to reduce the GHG-, Hydrocarbon (HC)-, Nitrogen oxides (NOx)-, Sulphur oxides (SOx)-, and particulate matter (PM) emissions. The Flettner rotor is a technology that utilizes wind and the Magnus effect to generate lift for propulsion assist of the vessel. This paper builds on recently reported findings demonstrating the viability of a Flettner rotor propulsion in a hybrid diesel-electric propulsion system for a small cargo ship. Prior related work provided CFD analyses to determine the optimal system architecture in terms of number of Flettner rotors, rotor sizing (diameter, length, etc.), rotation speed and direction, rotor(s) spacing, relative rotor(s) arrangement, etc. Optimal rotor rotational speed was determined to maximize the Lift-to-Drag (L/D) ratios for various geometric rotor configurations. Sample calculations for optimal operating conditions based on Flettner rotor geometry, rotational speed, wind speed, ship's velocity highlight the potential shipboard power contributions from the operation of Flettner rotor as a power-assist to total onboard propulsive ship power. Estimations of commensurate emissions reductions from engine exhaust (assuming a Diesel-powered main engine) support the estimated environmental benefits of the proposed hybrid Flettner rotor power-assisted propulsion architecture.
***Key words :*** Exhaust Gas Emissions Reduction; Flettner Rotor; Hybrid Ship Propulsion; System Integration; Wind-Assisted Propulsion Systems (WAPS)

## 1. INTRODUCTION

This paper illustrates a reduction of pollution from emissions present in the exhaust of heat engine (mainly Diesel cycle)-powered merchant ships, specifically, during operations of such ships both near, and in port. Typically, these (Diesel cycle) heat engines, burning hydrocarbon (HC) fuels, are predominantly used for main propulsion. Most of the hydrocarbon pollution reduction initiatives are focused on the emissions from larger heat engines used for main ship propulsion.

About 90% of the world's global trade is carried by large sea going vessels. Of these, the following three types are the highest fuel consumers on per annual basis: container ships, bulk carriers, and oil tankers. Combined, these types of ships consume nearly 2/3 (> 66%) of the annual global shipping fuel (HFO-equivalent) based on recent data analyses from Janes Sea Module Global Shipping Database [1].

According to current estimates presented in the Third IMO GHG Study 2014 [2], international shipping emitted 796 million tons of $CO_2$ in 2012, which accounts for no more than about 2.2% of the total emission volume for that year. Furthermore, the mid-range forecasted scenarios discussed during the Third IMO GHG Study 2014 showed that by 2050, $CO_2$ emission from international shipping could grow by between 50% and 250% depending on the expected future economic growth, world maritime commerce, and energy developments.

The Fourth IMO GHG Study 2020 [3] provided a global perspective for ocean-going vessels fuel consumption. This was consistent with the earlier findings based on the 2018 data from Janes Sea Module Global Shipping Database [1].

GHG emissions, which trap heat in the Earth's atmosphere, resulting in global warming thus leading to climate changes, consist of the following gases [4]: 79.7% Carbon Dioxide ($CO_2$), 11.1% methane ($CH_4$), 6.1% Nitrous oxide ($N_2O$), and trace amounts (3.1%) of Fluorinated gases, such as hydrofluorocarbons (HFCs), perfluorocarbons (PFCs), Sulphur hexafluoride ($SF_6$), and Nitrogen trifluoride ($NF_3$).

The international requirements on ship engines' emissions of NOx, SOx, and PM are determined and regulated by the IMO's document *MARPOL Convention*

Journal of Marine Technology and Environment
DOI:10.53464/JMTE.02.2026.08
ISSN (Print): 1844-6116
ISSN (Online): 2501-8795
https://www. jmte.eu

*Annex VI – Regulations for the Prevention of Air Pollution from Ships* [5]. These stringent requirements for NOx and SOx apply even close to shores within the Emission Control Areas (ECAs) for ship operations near land.

Energy Efficiency Design Index (EEDI) concept is an amendment to the IMO's MARPOL Annex VI [5], ensuring the reduction of GHG emissions from shipping. The EEDI principle is to compare the GHG emissions of new ships with a baseline of existing ships built during the 2000 – 2010 period. A reduction factor in the EEDI is required for all new ship builds.

The present work focused on the feasibility of the Flettner rotor power assist in augmenting ship propulsion in a hybrid diesel-electric power concept. This, in turn, demonstrated reductions in HC fuel consumption and commensurate decrease in HC-based airborne pollutants towards green (and/or "more-green") energy technologies to be implemented in ship propulsion systems. This is consistent with the IMO's recently announced goals for reducing shipping emissions: 40% compared to 2008 levels by 2030, and 70% by 2050.

## 2. AIRFOIL THEORY – LIFT AND DRAG

The current paper builds upon the earlier findings from a related previous work [6]. Detailed 2-D CFD analyses were completed with EasyCFD [7], a simple CFD teaching tool with a RANS *κ-ε* turbulence model. EasyCFD's built-in gas library was used to determine the air properties (at ambient conditions), with moderate mesh sizing (approx. 25,000 cells) for relatively fast processing. Denser meshing (auto-generated) was used near rotor's surface for higher resolution. Readers are directed to our previous work [6] for related details.

A rotating rotor (such as the Flettner Rotor) is similar to an aerofoil in producing lift, *L*, and drag, *D* (Fig. 1) while monitoring the value of *L/D* [8]. The lift, drag, and pitching moments of aerofoils, described by their respective section coefficients, $c_l$, $c_d$, and $c_m$, are functions of the angle of attack (AOA), *α*, and the operational speed of the aerofoil (i.e., the Reynolds number, *Re*. For a given *α* and *Re*, a typical aerofoil reaches its maximum lift at the maximum *α* beyond which it is assumed to be stalled due to separation of flow (where lift is rapidly lost, while drag is increasing).

Fundamental aerofoil theory [9] indicates that different aerofoil shapes (cross-sectional profiles) offer different lift-to-drag (*L/D*) ratios.

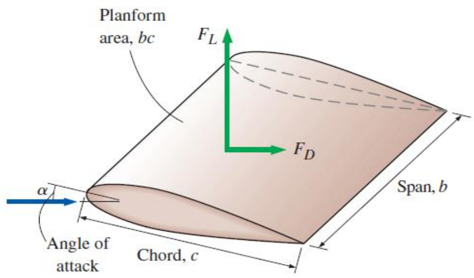


Figure 1. Typical aerofoil [8]

The Aspect Ratio, *AR* (i.e., span/chord) is an important wing performance characteristic relating lift and drag. Typically, higher *AR*s lead to higher *L/D* ratios but with more structural challenges (i.e., wing bending, wing tip deflection, wing root stresses, etc.). Lift and drag are defined in (1) and (2), respectively:

$$L = \frac{1}{2}\rho V^2 A C_L \quad (1)$$

$$D = \frac{1}{2}\rho V^2 A C_D \quad (2)$$

In our calculations we used well-established values for $C_L$ = 12.5 and $C_D$ = 0.2 from prior work [10]. The total lift coefficient, $C_L$, for a finite wing [11] is defined in (3).

$$C_L = \frac{(c_l)^2}{1+\frac{c_l}{\pi\,(AR)}} \quad (3)$$

Similarly, for modest values of *α*, the induced drag coefficient, $C_{D,i}$, and the total drag coefficient, $C_D$, are defined in (4) and (5), respectively.

$$C_{D,i} = \frac{(C_L)^2}{\pi\, e\, AR} \quad (4)$$

$$C_D = c_d + C_{D,i} \quad (5)$$

According to Prandtl Lifting Line Theory [9], an elliptical oval represents an ideal wing planform are (which minimizes induced drag through reduced wing downwash). In (4), *e* is the span efficiency factor, which is an index of how ideal a wing planform is, compared to the ideal elliptical oval shape.

A rotating rotor (such as the Flettner Rotor) is similar to an airfoil in producing lift, *L*, and drag, *D* while monitoring the value of *L/D*. A symmetric aerofoil, such as the NACA 0024 [12] produces no lift at *α* = 0 deg. (Fig. 2). The values of $C_L/C_D$ for the NACA 0024 aerofoil (Fig. 2) are given as function of several different Re numbers (i.e., 100,000; 200,000; 500,000; 1,000,000). $C_L/C_D$ ratio increases progressively with higher Re number. The corresponding maximum value for $C_L/C_D$ = 68.8 at *Re* = 1,000,000 occurs at α = 9 deg.

Journal of Marine Technology and Environment
DOI:10.53464/JMTE.02.2026.08
ISSN (Print): 1844-6116
ISSN (Online): 2501-8795
https://www.jmte.eu

Values for $C_L/C_D$ are lower for the lower *Re* values, respectively.

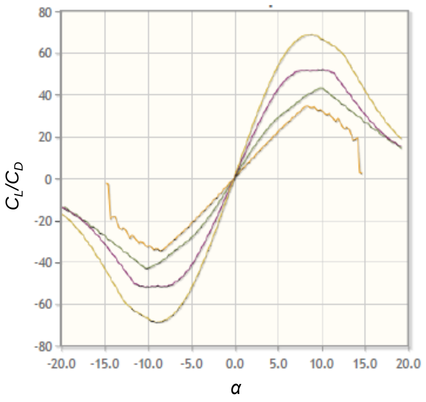


Figure 2. $C_L/C_D$ vs. α for NACA 0024 airfoil [12]

In our calculations for the Flettner Rotor, we used $C_L/C_D$ = 12.5/0.2 = 62.5, which is similar (within approx. 9%) to the maximum value of $C_L/C_D$ (at α = 9 deg.) for the NACA 0024 symmetric aerofoil profile.

## 3. RELATIVE WIND CALCULATIONS

Due to the motion of a ship with velocity $V_{ship}$, relative to the true wind, $V_{true}$, the apparent wind speed, $V_a$, creates an angle $\beta$ between the $L$ and $D$ force vectors for any true wind speed (and resulting apparent wind speed) direction (Fig. 3).

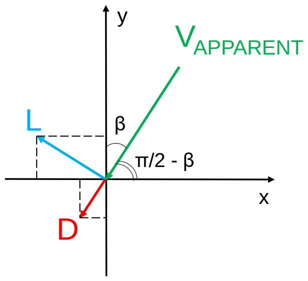


Figure 3. Basic Directions of Wind Relative to Ship

Considering the component of $L$ (10) in the y-direction (Fig. 4) and the component of D (11) in the y-direction (Fig. 5):

$$L_y = L\cos\left(\frac{\pi}{2} - \beta\right) \#(10)$$

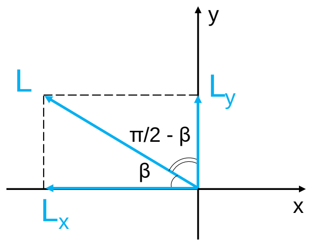


Figure 4. Lift Force Components

$$D_y = D\sin\left(\frac{\pi}{2} - \beta\right) \#(11)$$

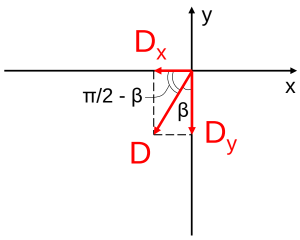


Figure 5. Drag Force Components

and summing only their components in the y-direction, we obtain:

$$F_{Thrust} = L\cos\left(\frac{\pi}{2} - \beta\right) - D\sin\left(\frac{\pi}{2} - \beta\right) \quad (12)$$

Substituting in the corresponding equations for Lift and Drag (Fig. 6) gives:

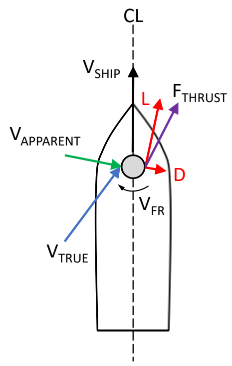


Figure 6. Basic wind directions and resultant forces vectors

$$F_{Thrust} = \frac{1}{2}\rho A V_a^2 [C_L(\sin\beta) - C_D(\cos\beta)] \ (13)$$

## 4. FLETTNER ROTOR POWER CALCULATIONS

Calculations yielded the expected power produced by a single Flettner Rotor in different wind speed and wind direction conditions to maintain a constant ship

Journal of Marine Technology and Environment
DOI:10.53464/JMTE.02.2026.08
ISSN (Print): 1844-6116
ISSN (Online): 2501-8795
https://www.jmte.eu

direction (heading) and speed. Additionally, the power required to rotate the Flettner Rotor was calculated (as electrical motor power consumption). This electrical motor power was then subtracted from the raw generated power by the Flettner Rotor. The remaining produced power by the Flettner Rotor is considered as replacement (or augmentation) power to the normally operating Diesel engine used to propel the ship along its charted heading and speed. The contributed power by the Flettner Rotor was compared to the total required ship propulsion power.

A set of calculations for a typical Flettner rotor application illustrates the expected benefits of the proposed hybrid propulsion system. Based on the total Lift and Drag due to the rotating Flettner Rotor, the power delivered by the Flettner Rotor (FR), $P_{L\&D}$ is shown in (14). The power, $P_{motor}$, consumed by an electric motor to rotate the FR is shown in (15).

$$P_{L\&D} = (L + D)V_{ship} \tag{14}$$

$$P_{motor} = \frac{1}{2}\rho A V_a^3 C_M \alpha \tag{15}$$

This power (15) is added as an additional load to the overall ship electrical load system. The power contribution from the FR, (i.e., "net power") to the overall ship power, $P_{FRprop}$ shown in (16).

$$P_{FRprop} = P_{L\&D} - P_{motor} \tag{16}$$

The assumed lift coefficient, $C_L$ = 12.5, and drag coefficient, $C_D$ = 0.2, were based on a prior study [10] The assumed moment coefficient, $C_M$ = 0.2, was based on the original work by Flettner [13].

In our work we modelled a Flettner Rotor with no end plates. Configurations using FRs with end plates will generally show improved results, hence, our initial assumptions are conservative.

The selected FR geometry is as follows:

*A* – vertical projected cross-sectional area of FR (i.e., *h x d*, *h* = FR height; *d* = FR diameter)

*h* = 35 m; *d* = 5 m; *h/d* = 7; *A* = *h x d* = 35 m x 5 m = 175 m$^2$;

*SR* – spin ratio $\alpha$ (ratio of FR surface tangential speed, $V_{FR}$, to apparent wind speed, $V_a$) = 0.5 – 4.0 (for a correlation of FR surface tangential speed, $V_{FR}$, to FR rotational speed, $\omega_{FR}$, please see Table 1). The formula used to convert from $V_{FR}$ (m/s) to $\omega_{FR}$ (rpm) is:

$$\omega_{FR} = \frac{V_{FR}}{0.5(FR_d)}(60) \tag{17}$$

A summary of results for a fixed $FR_h$ = 30 m, $FR_d$ = 5 m, *h/d* = 6, and variable surface tangential speeds, $V_{FR}$, is shown in Table 1. Conversion of ship speed, $V_{ship}$, true wind speed, $V_{true}$, or apparent wind speed, $V_a$, is done according to the relationship: 1 m/s = 1.9438 kn.

Table 1. Various operating speeds for FR installation

| | | | | Tangential | $V_{FR}$ / $V_a$ | | | | | Rotational |
|---|---|---|---|---|---|---|---|---|---|---|
| $V_{true}$, kn | $V_{true}$, m/s | $V_{ship}$, m/s | $V_a$, m/s | $V_{FR}$, m/s | *SR* | $FR_h$, m | $FR_d$, m | *h/d* | *A*, m$^2$ | $\omega_{FR}$, rpm |
| 11.7 | 6.0 | 4.5 | 1.5 | 5 | 3.33 | 30 | 5 | 6 | 150 | 120 |
| 14.6 | 7.5 | 4.5 | 3 | 10 | 3.33 | 30 | 5 | 6 | 150 | 240 |
| 17.5 | 9.0 | 4.5 | 4.5 | 15 | 3.33 | 30 | 5 | 6 | 150 | 360 |
| 20.4 | 10.5 | 4.5 | 6 | 20 | 3.33 | 30 | 5 | 6 | 150 | 480 |
| 23.3 | 12.0 | 4.5 | 7.5 | 25 | 3.33 | 30 | 5 | 6 | 150 | 600 |
| 26.2 | 13.5 | 4.5 | 9 | 30 | 3.33 | 30 | 5 | 6 | 150 | 720 |
| 29.2 | 15.0 | 4.5 | 10.5 | 35 | 3.33 | 30 | 5 | 6 | 150 | 840 |

$V_{ship}$ = ship's velocity vector; $V_{true}$ = true wind speed; $V_a$ = apparent wind speed = $V_{true}$ – $V_{ship;}$ $\rho$ – density of air (assume value at T = 20°C, 1 atm) = 1.205 kg/m$^3$; FR surface area = *h x π x d* = 35 m x π x 5 m = 549.8 m$^2$ ≈ 550 m$^2$.

Further assumptions for ship operational parameters include SFC = 180 g/kW-h using Bunker Heavy Fuel Oil (HFO) at a price of USD 650/ton. For the purpose a typical small general cargo ship (approx. 5500 dwt) was considered, operating at slow steaming speed. The resulting average ship propulsion power was approx. 1100 kW for average ship speed of 8.8 kn (4.5 m/s). The assumed average sea voyage distance was 2000 nm with an average voyage duration of approx. 10 days (240 h).

## 5. MOST LIKELY WIND SPEEDS (TRUE WIND SPEED) CALCULATIONS

A recent IMO publication [14] provides information on major global shipping routes (Ibid., Fig. 9) and statistical distribution of prevailing sea winds (Ibid., Fig. 10) along global shipping routes. Hence, consistent with this IMO guidance [14], the selected wind conditions (speeds) for our example were: $V_{true}$ = 10.5 m/s; $V_{ship}$ = 4.5 m/s; $V_a$ = $V_{true}$ — $V_{ship}$ = 6 m/s, for a Flettner rotor surface tangential speed $V_{FR}$ = 20 m/s; and a resulting spin ratio, SR = $V_{FR}$/$V_a$ = 20/6 = 3.33. Recalculating the resulting Lift, *L*, and Drag, *D*, forces, and resulting *L/D* ratio is shown in (18), (19), and (20), respectively.

$$L = \frac{1}{2}\rho A V_a^2 C_L = \frac{1}{2}\left[\left(1.205\frac{kg}{m^3}\right)(175m^2)\left(6\frac{m}{s}\right)^2(12.5)\right] = 47446.9\ N\#(18)$$

$$D = \frac{1}{2}\rho A V_a^2 C_D = \frac{1}{2}\left[\left(1.205\frac{kg}{m^3}\right)(175m^2)\left(6\frac{m}{s}\right)^2(0.2)\right] = 759.2\ N\#(19)$$

$$\frac{L}{D} = \frac{47446.9}{759.2} = 62.5 \tag{20}$$

The power delivered by the Flettner Rotor (FR), $P_{L\&D}$ is shown in (21). The power consumed by an electric motor to rotate the FR, $P_{motor}$ is shown in (22). Power contribution from the FR, $P_{FRprop}$ is shown in (23).

$$P_{L\&D} = (L + D)V_{Ship} = (47446.9\ N + 759.2\ N)\left(4.5\frac{m}{s}\right) = 216927.5\ W\#(21)$$

Journal of Marine Technology and Environment
DOI:10.53464/JMTE.02.2026.08
ISSN (Print): 1844-6116
ISSN (Online): 2501-8795
https://www. jmte.eu

$$P_{motor} = \frac{1}{2}\rho A V_a^3 C_M \alpha = \frac{1}{2}\left[\left(1.205\frac{kg}{m^3}\right)(175m^2)\left(6\frac{m}{s}\right)^3(0.2)(3.33)\right] = 15168\ W \#(22)$$

$$P_{FRprop} = P_{L\&D} - P_{motor} = 201.7\ kW \quad (23)$$

These results are consistent with recently published similar estimates (Fig. 3, p. 9 of [15]) for a ship using: $V_{ship}$ = 14 kn, $V_{true}$ = 10 m/s, $d/h$ = 4.76, $SR$ = 3.

Average power contribution (%) from FR, $P_{FRprop,\%}$, to total ship power demand, $P_{ship}$:

$$P_{FRprop,\%} = \left(\frac{PP_{FRprop,\%}}{P_{ship}}\right)100\% = \left(\frac{201.7}{1100}\right)100\% = 18.33\% \#(24)$$

## 6. SHIP ENGINE EMISSIONS REDUCTION CALCULATIONS

The annual reduction in emissions due to using Flettner Rotor ($AER_{FR}$) is calculated by Eq. 25 [16]:

$$AER_{FR} = \sum_{i=1}^{i=n} N_{FR}\, P_{FR} F_e H \#(25)$$

where:

$N_{FR}$ – number of FRs used; $P_{FR}$ – net power provided by FR(s) to main engine propulsion; $F_e$ – emission factors (energy based), g/kW-h; $H$ – sailing hours per year.

Exhaust emissions from marine diesel engines consist mostly of $N_2$, $O_2$, $CO_2$, $H_2O$ and with smaller quantities of CO, SOx, NOx, partially reacted/non-fully burned HCs and PM, as well as a group of trace pollutants named, known as micro pollutants. Next, we consider each of these emission species.

### *6.1 Exhaust gas emission species*

**NOx**

Oxides of Nitrogen resulting for the oxidation of molecular nitrogen ($N_2$) in the combustion chamber and partially due to incomplete combustion are grouped as "NOx" to include various compounds: nitric oxide (NO), dinitrogen dioxide ($N_2O_2$), nitrogen dioxide ($NO_2$), etc. In addition to their high toxicity, NOx emissions combined with volatile organic compounds (VOCs) result in photochemical reactions leading to increased tropospheric ozone ($O_3$) levels [17]. These increased tropospheric $O_3$ levels are detrimental to plant vegetation. Global warming is particularly affected by the depletion of stratospheric $O_3$, due to another NOx emission (from nitrous oxide, $N_2O$).

**SOx**

Oxides of Sulphur due to Sulphur content in combusted fuel are grouped under "SOx" [18] to include Sulphur monoxide (SO), Sulphur dioxide ($SO_2$), di-Sulphur monoxide ($S_2O$), and Sulphur trioxide ($SO_3$). Similar to NOx, $SO_2$ emissions are detrimental to plant vegetation. Emissions regulations for SOx are becoming more stringent as lower Sulphur content in marine fuels is demanded. Alternative ways to reducing SOx emissions have been discussed in regulation 14 of IMOs' MARPOL Annex VI legislation [5].

**CO**

Carbon monoxide (CO) formation is due to incomplete combustion (as function of excess oxidizer, among other parameters) in diesel engines. Typically, CO emissions are low, in well-maintained diesel engines. However, the CO's relative concentration can increase significantly when diesel engines are not running optimally (and/or are poorly maintained). CO emissions have adverse health effects on humans causing respiratory issues. The effect of CO on global warming is relatively small.

**$CO_2$**

Carbon dioxide ($CO_2$) emissions result from the fuel being burned in diesel engines. The quantity of fuel burned is proportional to the engine power, and on a global scale, this has been increasing as shipping traffic is growing steadily through recent years. $CO_2$ has received increased attention lately due to its role as a GHG and its effect on global warming. IMO's EEDI legislation (in effect since 2013) has mandated strict lower EEDI limits to newly built ships compared to existing ships' EEDI indexes. As the global economy relies on shipping for over 90% of its trade, increased shipping will lead to commensurately higher $CO_2$ emissions, which, in turn, will continue to impact negatively global warming.

**HC**

Hydrocarbon (HC) emissions, which include various combinations of C, H, O, N, and S, result from partially burned fuel in the diesel engine. The concentration of HC emissions is also dependent on the specific engine operational load. HC emissions can be involved in the formation of photochemical smog and tropospheric $O_3$ thus affecting global warming.

**PM**

Particulate matter (PM) emissions (generally regarded as "soot") resulting from incomplete (partial) combustion processes of HC fuels contain a mixture of inorganic and organic substances. In diesel engines, PM tend to be very small, in the order of sub-µm (i.e., < 1 x $10^{-6}$ m) in diameter, which contributes to their easy

Journal of Marine Technology and Environment
DOI:10.53464/JMTE.02.2026.08
ISSN (Print): 1844-6116
ISSN (Online): 2501-8795
https://www. jmte.eu

dispersal. Other versions of PM, as quantified by their statistically predominant diameter of approx. 10 μm (i.e., $PM_{10}$) have been characterized. The sooting tendency in combustion depends on the type of flames (i.e., premixed vs. diffusion), operational flame temperature (i.e., "cool" vs "hot), etc. It is a complicated process whose details are beyond the scope of this study. A detailed review has been published elsewhere [18].

**MPs**

The last (and smallest) group of emission pollutants, i.e., micro pollutants, consists of trace constituents (typically in ppb[1] levels), but which can still demonstrate sever adverse environmental effects even at these diminished concentrations. In the context of diesel engines emissions, micro pollutants include organic trace pollutants and heavy metals [17]. The organic micro pollutants include polyaromatic hydrocarbons (PAH), polychlorinated biphenyls (PCB), polychlorinated dibenzodioxins (PCDD), and polychlorinated dibenzofurans (PCDF). The group of heavy metals includes many transition metals[2] such as Cd, Cr, Cu, Hg, Ni and Zn; and some non-transition metals[3] such as Pb and the metalloids As and Se. Due to the very low (trace) amounts of these micro pollutants we will not consider them in our analyses. Further details in photochemistry of air pollution can be found elsewhere [19].

## 6.2 *Exhaust gas emission factors*

The following values for exhaust gas emission factors, $F_e$, were used (in units of g/kW-H): NOx = 18.1; SOx = 10.29; CO = 1.4; $CO_2$ = 620.62; HC = 0.6; PM = 1.42 [16]. These annual emissions reduction values (AER) appeared to be consistently updated from the earlier AER values [20]: NOx = 17; SOx = 10; CO = 1.4; $CO_2$ = 655; HC = 0.6; PM = 1.25. In this same earlier work [20], the AER value for SOx was based on an assumed average fuel-sulphur content of 2.5% for HFO.

Compared to the above emission values for NOx (rather dated at 18.1 g/kW-h), IMO's NOx limits have been dropping considerably from 17.0 g/kW-h (2000) to about 3.4 g/kW-h (2016), and with a continued tendency to further restrictions [21]. These NOx weighted cycle emission limits are based on ship engine's rated speed (rpm). In our case, we have selected the NOx limits for large 2-cycle turbocharged crosshead diesel engines, with rated speeds under 130 rpm. At the same time, marine engine makers have been developing strategies for newly built ships (post-2000) to comply with IMO's stringent limits by introducing water in the combustion chamber, or by humidifying the intake air (approx. 4 g/kW-h). Further NOx reductions are achieved by applying Selective Catalytic Reactor (SCR) technologies [22] to reach even lower emissions (< 2 g/kW-h).

## 6.3 *Global ship utilization*

Global merchant ships utilization generally varies with prevailing global freight rates. Assuming low freight rates, hence low annual ship utilization (say, 60%), i.e., 5256 engine hours/year, or high freight rates, hence high annual ship utilization (80%), i.e., 7008 engine hours/year, one can choose an appropriate estimated average of, say, 70% annual ship utilization, i.e., 6132 engine hours/year. These values are generally consistent with the prior estimates [20] of 5500, 6500, and 7010 engine hours/year. In our example we use the average value of 6500 engine hours/year. This is a reasonable average value of (approx. 70%) annual ship utilization consistent with prior works [23].

More detailed analyses [24] based on geographic specification of global ship activities and average annual usage derived from the publicly available International Comprehensive Ocean-Atmosphere Data Set (ICOADS) and the U.S. Coast Guard's own data set Automated Mutual-Assistance Vessel Rescue System (AMVER) were, in general, consistent with the earlier findings [23]. Furthermore, these authors [23] adjusted their estimates for average annual ship utilization accordingly based on related feedback from colleagues [25].

## 6.4 *Reductions in ship main engine exhaust emissions - example*

Calculations for the reduction in each of the emissions species separately (on an annual basis), NOx, SOx, CO, $CO_2$, HC, and PM are shown in equations (26), (27), (28), (29), (30), and (31), respectively.

$$\sum_{i=1}^{i=n} N_{FR}\, P_{FR} F_e H = (1)(201.7\ kW)\left(18.1\ \frac{g}{kW-h}\right)(6500\ h)\left(\frac{1\ ton}{1\ x\ 10^6\ g}\right) = 23.73\ tons \quad \#(26)$$

$$\sum_{i=1}^{i=n} N_{FR}\, P_{FR} F_e H = (1)(201.7\ kW)\left(10.3\ \frac{g}{kW-h}\right)(6500\ h)\left(\frac{1\ ton}{1\ x\ 10^6\ g}\right) = 13.51\ tons \quad \#(27)$$

$$\sum_{i=1}^{i=n} N_{FR}\, P_{FR} F_e H = (1)(201.7\ kW)\left(1.4\ \frac{g}{kW-h}\right)(6500\ h)\left(\frac{1\ ton}{1\ x\ 10^6\ g}\right) = 1.84\ tons \quad \#(28)$$

$$\sum_{i=1}^{i=n} N_{FR}\, P_{FR} F_e H = (1)(201.7\ kW)\left(620.62\ \frac{g}{kW-h}\right)(6500\ h)\left(\frac{1\ ton}{1\ x\ 10^6\ g}\right) = 813.66\ tons \quad \#(29)$$

$$\sum_{i=1}^{i=n} N_{FR}\, P_{FR} F_e H = (1)(201.7\ kW)\left(0.6\ \frac{g}{kW-h}\right)(6500\ h)\left(\frac{1\ ton}{1\ x\ 10^6\ g}\right) = 0.79\ tons \quad \#(30)$$

[1] ppb = parts per billion, i.e., 1 x $10^{-9}$ concentration

[2] Transition metals are found in the "d-block" of the Periodic Table (groups 3 to 12)

[3] Non-ttransition metals are found in the "s-block" (groups 1 and 2) and "p-block" (groups 13 to 18) of the Periodic Table

Journal of Marine Technology and Environment
DOI:10.53464/JMTE.02.2026.08
ISSN (Print): 1844-6116
ISSN (Online): 2501-8795
https://www.jmte.eu

$$\sum_{i=1}^{i=n} N_{FR} P_{FR} F_e H = (1)(201.7\ kW)\left(1.42\ \frac{g}{kW-h}\right)(6500\ h)\left(\frac{1\ ton}{1\ x\ 10^6\ g}\right) = 1.86\ tons \quad \#(31)$$

The effects of using one Flettner Rotor for a ship speed of 4.5 m/s (8.8 kn.), for various wind direction angles (0° – 360°) on the annual emissions reduction are shown in Fig. 7 ($CO_2$), Fig. 8 (NOx (upper trace) and SOx (lower trace)), and Fig. 9 (CO (upper trace) and HC (lower trace)). Due to some uncertainty in the estimated and measured approaches for PM, no PM data were plotted. In general, however, annual PM emissions reduction followed closely the CO emissions reduction curve (Fig. 9, upper trace).

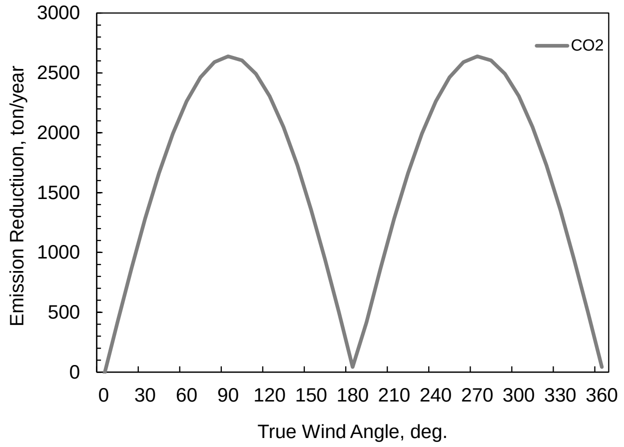


Figure 7. $CO_2$ Emissions Reduction

The highest emissions reduction occurs at true wind speed angles of approx. 90° and 270°. This is consistent with the occurrence of the FR's maximum lift force and resulting net output power along the intended movement direction (heading) of the ship. Even at close angles to the wind (close-hauled), at say, 25°-35°, and at high angles before the bind (running), at say, 145°-155°, the emissions reduction is already significant (across all emission species). Conversely, the lowest emissions reduction is shown near 0° (head wind) and 360° (tail wind).

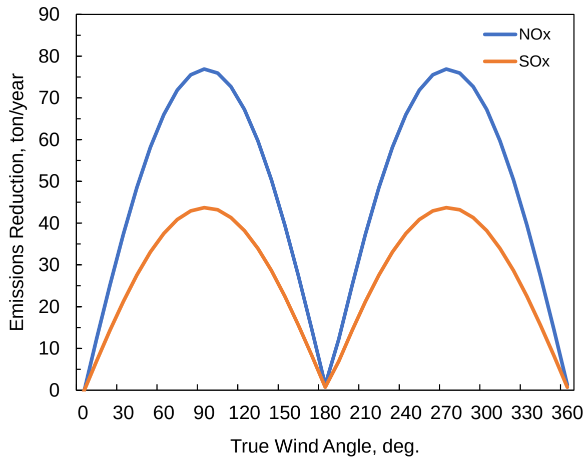


Figure 8. NOx and SOx Emissions Reductions

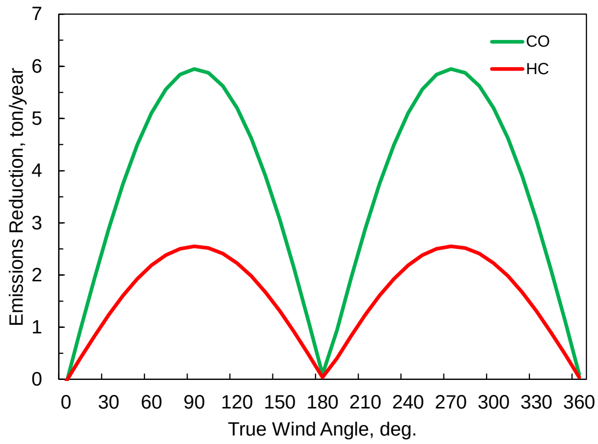


Figure 9. CO and HC Emissions Reductions

In these instances, the sensible operational suggestion may be to depower (and/or stow away where possible) the Flettner Rotor and operate the ship entirely on diesel power. At these true wind directions (0° and 360°) there is no effective power extracted by the Flettner Rotor as shown in the previous related work [6].

Journal of Marine Technology and Environment
DOI:10.53464/JMTE.02.2026.08
ISSN (Print): 1844-6116
ISSN (Online): 2501-8795
https://www.jmte.eu

## 7. CONCLUSIONS

Consistent with our prior work CFD analyses, a directly proportional relationship between Flettner rotor rotational speed and resulting lift was confirmed. The resulting optimal L/D ratio appears to be optimized at true wind speeds of approx. 10 to 15 m/s.

For a typical predominant true wind speed of about 10.5 m/s, we demonstrated optimal performance and significant reduction in exhaust emissions (near true wind speed angles of approx. 90° and 270°) form a typical Diesel main engine, when an operational Flettner rotor is used in a hybrid mode application (Diesel-electric propulsion).

## 8. ACKNOWLEDGMENTS

The author welcomes any related comments on improving the contents of this paper, as well as suggestions for any future related follow-on papers.

## 9. CREDIT AUTHORS STATEMENT

Conceptualization: R.L.; Investigation: R.L.; Methodology: R.L.; Resources: R.L.; Visualization: R.L.; Writing – original draft: R.L.; Writing – review & editing: R.L.

## 9. REFERENCES

[1] *Janes Sea Module Global Shipping Database*, 2024, May 13, https://customer.janes.com/portal/Account/PreAuthenticate?callingurl=https%3A%2F%2Fcustomer.janes.com%2

[2] Smith, T.W.P., et al., 2105, *Third IMO Greenhouse Gas Study 2014* – Executive Summary and Final Report, London, UK.

[3] Fiber, J. et al., 2021, *Fourth IMO GHG Study 2020* – Executive Summary and Final Report, London, UK.

[4] *EPA. United States Environmental Protection Agency. Overview of Greenhouse Gases*, 2026, April 27, https://www.epa.gov/ghgemissions/overview-greenhouse-gases

[5] MARPOL, 1997, *Annex VI*, IMO, London, UK.

[6] Almadani, Z., Garcia-Billings, J., Newsom, H., Ribarov, L.A., 2023, Flettner Rotor-Powered Marine Vessel – Design Evaluation and Systems Optimization. *Sustainability in Ship Design and Operations (SISDO 2023) Conference*, Glen Cove, NY.

[7] Lopes, A. M. G., 2016, A 2D Software System to Expedite Analysis of CFD Problems in Complex Geometries. *Comp. Appl. Eng. Educ.*, 24(1), 27–38

[8] Çengel, Y.A., Cimbala, J.M., 2014, *Fluid Mechanics*. 4th ed. McGraw Hill, New York, NY, USA.

[9] Anderson, J.D., 2005, *Introduction to Flight*. McGraw-Hill Education, New York, NY, USA.

[10] Craft, T.J., Iacovides, H., Johnson, N., Launder, B., 2012, Back to the Future: Flettner-Thom Rotors for Maritime Propulsion? *Turb., Heat and Mass Trans.*, (7), 1–10.

[11] Houghton, E.L., Carpenter, P.W., 2003, *Aerodynamics for Engineering Students*. Butterworth-Heinemann, Oxford, UK.

[12] Airfoil Tools (NACA 0024) – Cl/Cd v Alpha http://airfoiltools.com/airfoil/details?airfoil=naca0024-il

[13] Flettner, A., 1926, *Mein Weg zum Rotor. ("The Story of the Rotor") MIT 114 ABB. Verlag Koehler & Amelang, Leipzig 1926. 123 S*. ZAMM - Journal of Applied Mathematics and Mechanics / Zeitschrift Für Angewandte Mathematik Und Mechanik, 6(6), 505–505. doi.org/10.1002/zamm.19260060625.

[14] *IMO MEPC.1/Circ.896*, 2021, London, UK.

[15] Vigna, V., Figari, M., 2023, *Wind-Assisted Ship Propulsion: Matching Flettner Rotors with Diesel Engines and Controllable Pitch Propellers*. J. Mar. Sci. Eng., 11(1072), 1–18.

[16] Seddiek, I., Ammar, N.R., 2021, *Harnessing Wind Energy on Merchant Ships: Case Study Flettner Rotors onboard Bulk Carriers*. Env. Sci. and Pollution Res., (28), 32695–32707.

[17] Kristiansen, H.O., 2017, *Energy Demand and Exhaust Gas Emissions of Marine Engines. Project no. 2016-108: Update of Decision Support System for Exhaust Gas Emissions Calculations*. Report no.5. Technical University of Denmark (DTU).

[18] Glassman, I., 1996, *Combustion*. 3rd ed. Academic Press, San Diego, CA, USA.

[19] Leighton, P.A., 1961, *Photochemistry of Air Pollution*. Academic Press, New York.

Journal of Marine Technology and Environment
DOI:10.53464/JMTE.02.2026.08

ISSN (Print): 1844-6116
ISSN (Online): 2501-8795
https://www. jmte.eu

[20] Corbett, J.J., Koehler, H.W., 2003, *Updated Emissions from Ocean Shipping*. J. of Geophys. Res., 108(D20):4650, doi:10.1029/2003JD003751.

[21] IMO Nitrogen Oxides (NOx) – Regulation 13 (https://www.imo.org/en/OurWork/Environment/Pages/Nitrogen-oxides-(NOx)-%E2%80%93-Regulation-13.aspx).

[22] Koehler, H.W., 2003, *NOx Emissions from Merchant Ships*. Marine Reporter & Eng. News, (June 2003), 68-70.

[23] Corbett, J.J., Koehler, H.W., 2004, *Considering Alternative Input Parameters in an Activity-Based Ship Fuel Consumption and Emission Model: Reply to Comment by Øyvind Endersen et al on "Updated Emissions from Ocean Shipping*." J. of Geophys. Res.,109(D23303):4650,doi:10.1029/2004JD005030.

[24] Endresen, Ø, Søgård, E., Sundet, J.K., Dalsøren, S.B., Isaksen, I.S.A., Berglen, T.F., Gravir, G., 2003, *Emission from International Sea Transportation and Environmental Impact*. Journal of Geophysical Research, 108(D17), 4560. doi:10.1029/2002JD002898.

[25] Endresen, Ø, Søgård, E., Bakke, J., Isaksen, I.S.A., 2004, *Substantiation of a Lower Estimate for the Bunker Inventory: Comment on "Updated Emissions from Ocean Shipping*" by J. J. Corbett and H.W. Koehler. J. of Geophys. Res., 109(D23302), 4560. doi:10.1029/2004JD004853.